Effects of dielectric discontinuities on two charged plates

Y. S. Jho,[1,2,*] G. Park,[3] C. S. Chang,[1,3] P. A. Pincus,[1,2] and M. W. Kim[1,2]
[1]*Department of Physics, Korea Advanced Institute of Science and Technology, Yuseong-Gu, Daejeon, Korea 305-701*
[2]*Materials Research Laboratory, University of California at Santa Barbara, Santa Barbara, California*
[3]*Courant Institute of Mathematical Sciences, New York University, 251 Mercer Street, New York, New York 10012, USA*
(Received 10 November 2006; revised manuscript received 10 May 2007; published 26 July 2007)

Counterions in a biological system are charged in water and interact with charged macroions, which are generally made up of hydrocarbons. The dielectric difference between water and the hydrocarbon substrates occurs naturally, and may greatly affect the electrostatic properties of biological systems. Particularly for a slab geometry, bulk counterions that are dissolved in water are driven to the midplane of the slab because of their repulsive interaction with their image charges. The pressure between two charged plates becomes less repulsive since the low dielectric constant of the hydrocarbon substrate creates stronger association between counterions and surface charges as compared to the case of no dielectric discontinuity.

DOI: 10.1103/PhysRevE.76.011920 PACS number(s): 87.10.+e, 61.20.Ja, 68.47.Pe, 82.39.Rt

I. INTRODUCTION

One of the fundamental forces that govern the behavior of biological systems is the Coulomb interaction. Many phenomena in biological systems (for example, interacting polyelectrolytes, transport across membranes, and polymer adsorption and desorption kinetics at membranes) have been successfully described on the basis of the Coulomb interaction. These biological systems have a common trait in that they are composed of charged macroanions and counterions. For planar macroanions, these systems are often modeled as uniformly charged anion plates in the presence of pointlike counterions [1–8]. In our previous paper [9], we demonstrated that the discreteness of surface charge in a strong-coupling regime, which is more realistic than the uniform surface charge approximation, plays an important role in determining the counterion density profile and the nature of interaction between two surfaces. The surface charge discreteness enhances the localization of counterions to the surface, and results in stronger attraction between two plates. It was also found that the strong-coupling theory is effective in explaining the behavior of the discrete surface charge system in a strong-coupling regime.

These previous studies assumed, however, that the counterions and macroions are embedded in the same dielectric material. On the contrary, real biological systems contain counterions which are solubilized in water, while the surface charges are generally located on hydrocarbon substrates. The dielectric constant of water is 79 and that of the hydrocarbon substrate is 2; thus, a large difference of dielectric constant exists between water and hydrocarbon. Several studies showed that this dielectric difference could change the system characteristics significantly [10–16].

Menes *et al.* studied how the dielectric difference modifies charge-fluctuation-induced attraction. They showed that the interactions depend, in a nontrivial way, on the dielectric constants of the membrane and water, and different scaling with distance arises according to these properties [10]. Moreira and Netz studied the change of density distribution under dielectric discontinuity for the one-plate case [11]; the Hamiltonian of the system is changed from that in the case of no dielectric discontinuity. Additional interaction between charges and their images must be taken into account. Moreira and Netz found that counterions are driven away from a wall in the presence of a dielectric discontinuity, due to the repulsive interaction between counterions and their images. Nguyen *et al.* also showed that charge inversion phenomena can be explained by the large dielectric difference. They used image charges in the context of the dielectric difference between water and membrane [12,13]. Netz and Joanny calculated the adsorption of semiflexible polyelectrolytes considering dielectric contrast. They showed that image charge effects, which come from the dielectric discontinuity, make the polymer steep [14,15]. Andelman and Joanny demonstrated that the additional repulsive interaction due to the dielectric discontinuity can compete with the adsorption mechanism [16].

The goal of this paper is to study the effects of dielectric discontinuity between two plates in a slab geometry. The cases under current consideration are different from the one plate case. In a slab geometry, an infinite series of image charges should be fully accounted for to satisfy both boundary conditions. The main aim of the present study is to clarify the mechanism by which the interaction between two plates and the density distribution of counterions are modified in the presence of a dielectric discontinuity, compared to those calculated assuming no dielectric discontinuity. Previous results have already shown that there are various significant physical parameters, for example, counterion valence, phase, depth of surface charges, etc., which greatly influence the charge distribution and pressure between two plates. In this paper, these features are studied in detail in the presence of the dielectric discontinuity. Counterions are driven to midplane due to the repulsive interaction with their images. These phenomena are very noticeable when the radii of bulk counterions and surface charges are small and the dielectric constant of the surface medium is low. The pressure becomes less repulsive because of the low dielectric constant of the surface medium.

*joys@kaist.ac.kr

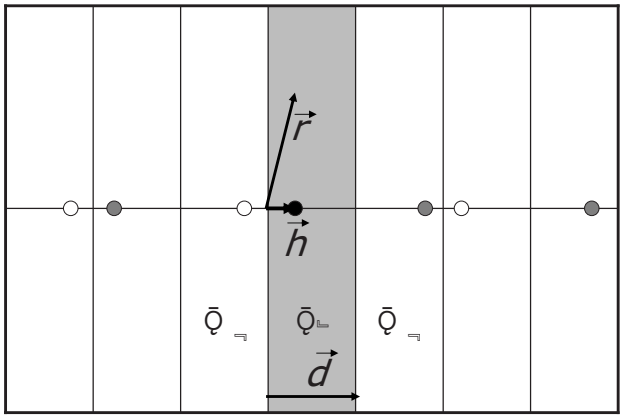

FIG. 1. Image charge picture for slab geometry: Original charge induces replicated image charges via both interfaces.

The remainder of this paper is composed as follows. In Sec. II, the numerical method for our study is described. In Sec. III, the counterion density profile and pressure between two surfaces are numerically measured while varying the system conditions (i.e., counterion valences), and compared with those in the case where there is no dielectric difference. Section IV provides a summary and concluding remarks.

II. INTERACTION BETWEEN TWO DIELECTRIC SLABS

A. Image charge method for a dielectric slab

The electrostatic potential of two particles can no longer be simply written as $1/r$ when dielectric discontinuity exists between the bulk and surface media. In this case, the image charge method can be applied to find a solution that satisfies the boundary conditions at both interfaces. Image charges are generated at two discontinuous interfaces, and the generated images are reflected again to the opposite interfaces and make two more image charges, and so on. This process is repeated infinitely, and finally the Hamiltonian of the system is described by an infinite summation of the interactions of the image charges. The electrostatic potential is described differently depending on the location of the charge. If the charges are located inside the slab, there will be two infinite series of image charges; conversely, if the charges are located outside the slab, there will be only one infinite series of image charges. In other words, if the charge is inside the slab, two infinite series of image charges occur with respect to both interfaces, while when the charge is located outside the slab, only one image charge is generated near the close interface and one infinitely replicated series of image charges with respect to the far interface.

Figure 1 shows a schematic of the model system. The dark region in the center represents the bulk medium, corresponding to water in view of our interest. The white region outside represents the surfaces, indicating a hydrocarbon substrate. The potential energy at $\vec{r}$ due to a charge at $\vec{h}$ can be expressed as the summation of the potentials that arise from the interaction between the charge and all of its images [17,18]. As mentioned above, the potentials are described differently depending on the location of the source charges and the location of the measuring points. There are two separate cases of interaction according to the location of the source particles, and three different cases for each of them can be differentiated as the location of the evaluation points is varied. If d is the separation of the two plates and z is the distance from one plate, then $\varphi(\vec{r})$ is the electrostatic potential at $\vec{r}$.

In case 1, a charge is inside the slab. For $z<0$,

$$\varphi(\vec{r}) = \frac{2}{\epsilon_1+\epsilon_2}\left(\sum_{l=0}^{\infty}\epsilon_{21}^{2l}\frac{1}{|\vec{r}-\vec{h}-2l\vec{d}|}+\sum_{l=1}^{\infty}\epsilon_{21}^{2l-1}\frac{1}{|\vec{r}+\vec{h}-2l\vec{d}|}\right). \tag{1}$$

For $0<z<d$,

$$\varphi(\vec{r}) = \frac{1}{\epsilon_2}\left(\frac{1}{|\vec{r}-\vec{h}|}+\sum_{l=0}^{\infty}\epsilon_{21}^{2l+1}\frac{1}{|\vec{r}+\vec{h}+2l\vec{d}|}+\sum_{l=1}^{\infty}\epsilon_{21}^{2l}\frac{1}{|\vec{r}-\vec{h}-2l\vec{d}|}+\sum_{l=1}^{\infty}\epsilon_{21}^{2l-1}\frac{1}{|\vec{r}+\vec{h}-2l\vec{d}|}+\sum_{l=1}^{\infty}\epsilon_{21}^{2l}\frac{1}{|\vec{r}-\vec{h}+2l\vec{d}|}\right). \tag{2}$$

For $z>d$,

$$\varphi(\vec{r}) = \frac{2}{\epsilon_1+\epsilon_2}\left(\sum_{l=0}^{\infty}\epsilon_{21}^{2l}\frac{1}{|\vec{r}-\vec{h}+2l\vec{d}|}+\sum_{l=0}^{\infty}\epsilon_{21}^{2l+1}\frac{1}{|\vec{r}+\vec{h}+2l\vec{d}|}\right). \tag{3}$$

In case 2, a charge is present outside the slab, i.e., in the background medium. When a charge is outside the left substrate, for $z<0$,

$$\varphi(\vec{r}) = \frac{1}{\epsilon_1}\left[\frac{1}{|\vec{r}-\vec{h}|}+\epsilon_{12}\frac{1}{|\vec{r}+\vec{h}|}-\frac{4\epsilon_1\epsilon_2}{(\epsilon_1+\epsilon_2)^2}\sum_{l=1}^{\infty}\left(\epsilon_{12}^{2l-1}\frac{1}{|\vec{r}+\vec{h}-2l\vec{d}|}\right)\right]; \tag{4}$$

for $0<z<d$,

$$\varphi(\vec{r}) = \frac{2}{\epsilon_1+\epsilon_2}\left(\sum_{l=0}^{\infty}\epsilon_{12}^{2l}\frac{1}{|\vec{r}-\vec{h}+2l\vec{d}|}-\sum_{l=1}^{\infty}\epsilon_{12}^{2l-1}\frac{1}{|\vec{r}+\vec{h}-2l\vec{d}|}\right); \tag{5}$$

for $z>d$,

$$\varphi(\vec{r}) = \frac{4\epsilon_2}{(\epsilon_1+\epsilon_2)^2}\sum_{l=0}^{\infty}\epsilon_{12}^{2l}\frac{1}{|\vec{r}-\vec{h}+2l\vec{d}|}. \tag{6}$$

Otherwise, when a charge is outside the right substrate, for $z>d$,

$$\varphi(\vec{r}) = \frac{1}{\epsilon_1}\left[\frac{1}{|\vec{r}-\vec{h}|} + \epsilon_{12}\frac{1}{|\vec{r}+\vec{h}-2\vec{d}|} - \frac{4\epsilon_1\epsilon_2}{(\epsilon_1+\epsilon_2)^2}\sum_{l=1}^{\infty}\left(\epsilon_{12}^{2l-1}\frac{1}{|\vec{r}+\vec{h}+2(l-1)\vec{d}|}\right)\right]; \quad (7)$$

for $0<z<d$,

$$\varphi(\vec{r}) = \frac{2}{\epsilon_1+\epsilon_2}\left(\sum_{l=0}^{\infty}\epsilon_{12}^{2l}\frac{1}{|\vec{r}-\vec{h}-2l\vec{d}|} - \sum_{l=1}^{\infty}\epsilon_{12}^{2l-1}\frac{1}{|\vec{r}+\vec{h}+2(-1)\vec{d}|}\right); \quad (8)$$

for $z<0$,

$$\varphi(\vec{r}) = \frac{4\epsilon_2}{(\epsilon_1+\epsilon_2)^2}\sum_{l=0}^{\infty}\epsilon_{12}^{2l}\frac{1}{|\vec{r}-\vec{h}-2l\vec{d}|}. \quad (9)$$

Here, $\vec{r}$ is the point at which the potential is measured, and $\vec{h}$ denotes the position of the source. Here, ϵ_1 indicates the dielectric constant of the outer surface media, and ϵ_2 that of the inserted bulk medium. Note that ϵ_{12} and ϵ_{21} are defined as $\epsilon_{12}=(\epsilon_1-\epsilon_2)/(\epsilon_1+\epsilon_2)$ and $\epsilon_{21}=(\epsilon_2-\epsilon_1)/(\epsilon_2+\epsilon_1)$. These parameters are important because they represent the properties of the dielectric discontinuity, i.e., the sizes of the image charges that can be induced from the original real charge. ϵ_{21} becomes positive when $\epsilon_2>\epsilon_1$, meaning that an image charge of the same sign is induced by the dielectric discontinuity. As a result, a repulsive interaction exists between the counterions and the dielectric medium. On the other hand, when $\epsilon_2<\epsilon_1$, oppositely signed image charges are induced by the dielectric discontinuity. This case resembles the situation where the real charge is located in a vacuum that is bounded by metal; the charge in that case tends to be moved to the boundary due to the attraction that originates from its image charges. These series converge because $|\epsilon_{21}|$ and $|\epsilon_{12}|$ are always less than 1.

B. Explicit calculation of potential

The electrostatic layer correction (ELC) method [19–21] was originally invented to apply three-dimensional (3D) periodic field calculation methods to the two-dimensional periodic slab $(2D+h)$ geometry. It transforms the slowly converging infinite series of summation to rapidly decaying series. The ELC method is a good way of accounting for a charge contribution from replicated layers. The potential of infinitely replicated image charges has the same structure, and the ELC is applicable to this kind of system [21]. The potential for a square lattice is expressed as follows:

$$\phi(\vec{r}) = \sum_{m,n\in\mathcal{Z}}\varphi(\vec{r}+mL_x\hat{x}+nL_y\hat{y}), \quad (10)$$

where L_x and L_y denote the lengths of periodic domains in x and y. Then each term that corresponds to a layer decays exponentially with an increasing modulation number,

$$\sum_{m,n\in\mathcal{Z}}\frac{1}{|\vec{r}+mL_x\hat{x}+nL_y\hat{y}|} = \frac{4}{L_xL_y}\sum_{m>0,n>0}\frac{e^{-2\pi f_{mn}|z|}}{f_{mn}}\cos(\omega_m x)\cos(\omega_n y) + \frac{2}{L_xL_y}\sum_{m>0}\frac{e^{-2\pi f_m|z|}}{f_m}\cos(\omega_m x) + \frac{2}{L_xL_y}\sum_{n>0}\frac{e^{-2\pi f_n|z|}}{f_n}\cos(\omega_n y) - \frac{2\pi}{L_xL_y}|z|, \quad (11)$$

where $\vec{r}=(x,y,z)$, $f_m=m/L_x$, $f_n=n/L_y$, $f_{mn}=\sqrt{(m/L_x)^2+(n/L_y)^2}$, $\omega_m=2\pi f_m$, and $\omega_n=2\pi f_n$. The last term remains constant since potentials that come from the left images of the original charge cancel with potentials coming from its right side. As a result, the potential depends only on d. For the case of interactions between surface charges, the last term is clearly constant. In addition, interactions between bulk particles depend only on d. This can be easily understand by rearranging the last terms of Eq. (11) as follows:

$$\sum_{l=0}^{\infty}\{\epsilon_{21}^{2l+1}(2ld+z+h)+\epsilon_{21}^{2l+1}[2(l+1)d-z-h]\} + \sum_{l=1}^{\infty}[\epsilon_{21}^{2l}(2ld-z+h)+\epsilon_{21}^{2l}(2ld+z-h)].$$

In a similar fashion, interactions between bulk and surface particles are also constant. $|z-h|$ or $|z+h|$ are less than d, and the sign of $|z\pm h\pm 2ld|$ depends on the value of l; i.e., $\mathrm{sgn}(\pm l)(z\pm h\pm 2ld)$ when $l\geqslant 1$.

We can decompose the whole series into the first few direct terms and ELC terms. Direct terms are calculated by the Leckner-Sperb method. However, the error of ELC terms is proportional to $e^{-2\pi m_c z/L_x}/L_x$ or $e^{-2\pi n_c z/L_y}/L_y$, where m_c and n_c represent the cutoff modes in the x and y directions. Hence, if d is small, it is better to include a few more terms in the direct summation. Let us rewrite the previous expression for the potential via the ELC method. We include terms $|z|<2d$ in Eq. (11) in the direct summation; for example, Eq. (1) becomes

$$\phi(\vec{r}) = \frac{2}{\epsilon_1+\epsilon_2}\left[\sum_{m,n>0}\left(\frac{1}{|\vec{r}-\vec{h}+mL_x\hat{x}+nL_y\hat{y}|} + \frac{\epsilon_{21}}{|\vec{r}+\vec{h}-2\vec{d}+mL_x\hat{x}+nL_y\hat{y}|}\right) + \sum_{m,n>0}\frac{4u_xu_y}{f_{mn}}\frac{e^{-2\pi f_{mn}(h-z)}+\epsilon_{21}e^{-2\pi f_{mn}(2d-h-z)}}{\epsilon_{21}^{-2}e^{4\pi f_{mn}d}-1} \times\cos\omega_m x\cos\omega_n y + \sum_{m>0}\frac{2u_xu_y}{f_m}\frac{e^{-2\pi f_m(h-z)}+\epsilon_{21}e^{-2\pi f_m(2d-h-z)}}{\epsilon_{21}^{-2}e^{4\pi f_m d}-1} \times(\cos\omega_m x+\cos\omega_m y)\right].$$

In addition to these pairwise interaction terms, self-energy should also be taken into account, since it is double the ordinary potential energy between different particles.

When z is located inside the slab, i.e., $0 \leqslant z \leqslant d$, Eq. (2) becomes

$$\phi(h) = \frac{1}{2\epsilon_2}\left[\sum_{m,n>0}\left(\frac{\epsilon_{21}}{|2h + mL_x\hat{x} + nL_y\hat{y}|} + \frac{\epsilon_{21}}{|2h - 2d + mL_x\hat{x} + nL_y\hat{y}|} + \frac{\epsilon_{21}^2}{|-2d + mL_x\hat{x} + nL_y\hat{y}|} + \frac{\epsilon_{21}^2}{|2d + mL_x\hat{x} + nL_y\hat{y}|}\right)\right.$$
$$+ \sum_{m,n>0}\frac{4u_xu_y}{f_{mn}}\frac{\epsilon_{21}e^{2\pi f_{mn}(-2h)} + \epsilon_{21}e^{-2\pi f_{mn}(2d-2h)} + 2\epsilon_{21}^2e^{-4\pi f_{mn}d}}{\epsilon_{21}^{-2}e^{4\pi f_{mn}d} - 1}\cos\omega_m x\cos\omega_n y$$
$$\left. + \sum_{m>0}\frac{2u_xu_y}{f_m}\frac{\epsilon_{21}e^{2\pi f_m(-2h)} + \epsilon_{21}e^{-2\pi f_m(2d-2h)} + 2\epsilon_{21}^2e^{-4\pi f_m d}}{\epsilon_{21}^{-2}e^{4\pi f_m d} - 1}(\cos\omega_m x + \cos\omega_m y)\right].$$

Other cases could also be similarly treated in a straightforward way, and hence are omitted here. If h is small, the direct summation should contain few lower modes.

III. RESULTS

Compared to the case of no dielectric discontinuity, two significant differences occur when a dielectric discontinuity is properly incorporated. One is the repulsive interaction that a counterion feels from the presence of image charges at the interfaces, and the other is the much stronger attraction between the surface and counterions arising from the low dielectric constant of the surface media.

As previously mentioned, the present study considers a system composed of water and a hydrocarbon substrate, the dielectric constants of which are 79 and 2, respectively. The amount of induced image charges is determined by ϵ_{21}, which incorporates the dielectric difference between the bulk and the surfaces. For charges in the higher dielectric regions, i.e., water, ϵ_{21} is positive. Thus the counterions experience image charges with the same sign. This leads to a repulsive interaction between the counterions and the surfaces. On the other hand, charges in the lower dielectric region, i.e., the hydrocarbon substrate, experience image charges with the opposite sign, and are therefore attracted to the interface.

Figure 2 shows the counterion density profile versus the surface dielectric constant where the depth D is $0.05a_\perp$ and $q=2$. Here, $a_\perp$ denotes the distance between surface charges, D denotes the depth of the surface charges, which is the sum of the radius of the surface charges and that of the counterions, and q is the valence of the counterions. In this study, the system conditions are $\Xi=5$, $d=6.7$ Å, and $a_\perp=22.35$ Å. Here, $\Xi \equiv q^2 l_B/\mu = 2\pi q^3 l_B^2 \sigma_0$, $\mu \equiv 1/(2\pi q l_B \sigma_0)$, $l_B = e^2/4\pi\epsilon_0\epsilon_2 k_B T$, and σ_0 is the average surface charge density. The radius of the counterions is taken to be half of that of the surface charges, and the surface charges are located on a square lattice with distance $a_\perp$ between the charges. A Monte Carlo simulation is performed [22,23]. Compared to the results of the case in which there is no dielectric discontinuity, the effects of the dielectric discontinuity make the midplane density higher while the density at the surface becomes smaller. When the dielectric constant of the surface medium is 2, then $\epsilon_{21}=77/81$. This large dielectric difference modifies the counterion localization at the surfaces. The position at which the counterion density is maximized is shifted to the center region, although the position was near the surface when no dielectric discontinuity effect was imposed. This is because the counterions are pushed to the center by the repulsive force between the counterions and their images in the presence of dielectric discontinuity. In order to measure the degree of this tendency, $n(d/2)/n(0)$ is defined to represent the ratio of the density at the midplane to that at the surfaces. This value remains less than 1, which means counterions are denser at the surface than the midplane, until $\epsilon_1 \simeq 20$. It becomes more than 1 at $\epsilon_1 \simeq 10$. When $\epsilon_1=2$, $n(d/2)/n(0)$ rises to 38.6 for the in-phase case. A similar tendency is observed in the out-of-phase case. However, the strength of $n(d/2)/n(0)$ in the out-of-phase case is weaker than that in the in-phase case. Specifically, it is about one-fourth of the strength of the in-phase case when $\epsilon_1=2$.

In Fig. 3, the system conditions correspond to those in Fig. 2, except that the depth is $0.3a_\perp$. Compared to the case of no dielectric discontinuity, the counterions are more weakly localized at the surface, because the strength of attraction between the surface charges and counterions be-

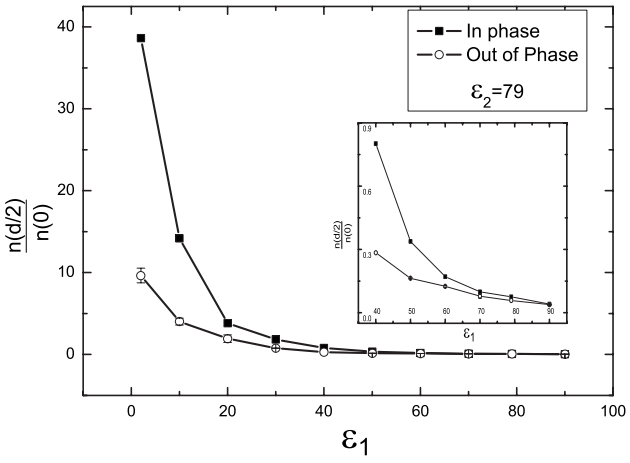

FIG. 2. Density ratio of counterions at midplane and at surfaces vs dielectric constant of the surfaces. $\Xi=5$, $q=2$, $D/a_\perp=0.05$, $r_c=D/3$, $d/a_\perp=0.133$.

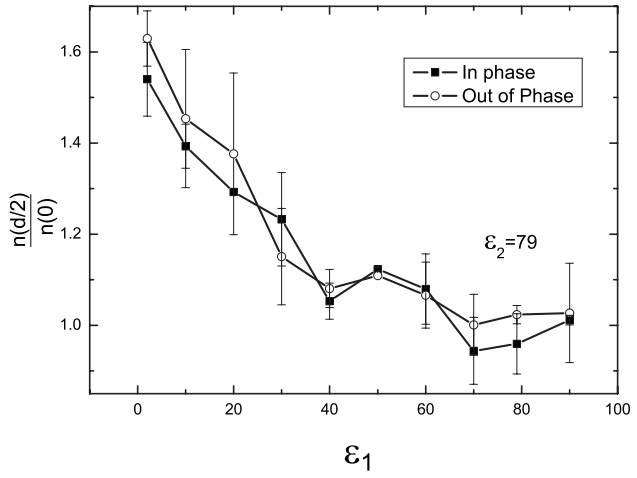

FIG. 3. Density ratio of counterions at midplane and at surfaces vs dielectric constant of the surfaces. $\Xi=5$, $q=2$, $D/a_\perp=0.3$, $r_c=D/3$, $d/a_\perp=0.133$.

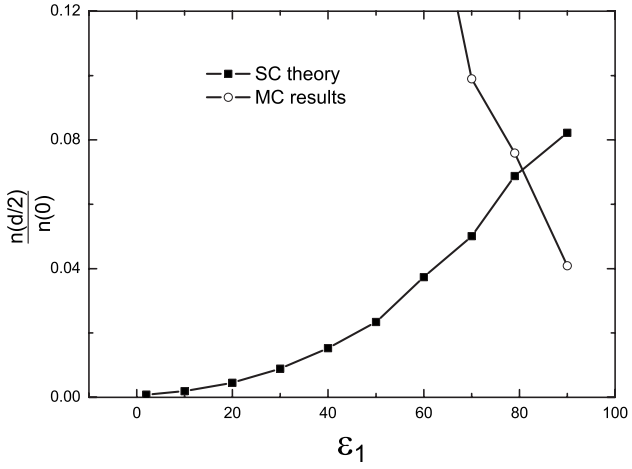

FIG. 4. Comparison of strong-coupling theory results with numerical simulations when there is dielectric discontinuity. $\Xi=5$, $q=2$, $D/a_\perp=0.05$, $r_c=D/3$, $d/a_\perp=0.133$.

comes smaller. Furthermore, the lateral correlation between them is weaker. Considering the dielectric discontinuity, a similar tendency with the previous case (counterions are driven to the center region) at low ϵ_1 is observed, but the strength of the interaction is much weaker. This could also be interpreted as a result of the weak interactions between surface charges and counterions. As a result, the ratio $n(d/2)/n(0)$ becomes smaller with increasing ϵ_1, but the rate of increase is much slower than in the case of $D=0.05a_\perp$.

In previous results, it was demonstrated that the strong-coupling theory is very successful in explaining simulation results in the presence of discrete surface charges with no dielectric discontinuity. However, in this case, the strong-coupling theory seems not to agree well with numerical results. In developing the strong-coupling theory, it was assumed that the electrostatic potential between charged particles would be represented as a Coulomb operator $1/r$. Therefore, the strong-coupling theory states that the density distribution of counterions depends only on the potential originating from the macroions,

$$\tilde{n}(\tilde{r}) \equiv \frac{n(\tilde{r})}{2\pi l_B \sigma_0^2} = \Lambda e^{-\tilde{u}(\tilde{r})} + O(\Xi^{-1}), \tag{12}$$

where $\tilde{u}(\tilde{r})$ is the potential due to macroions and the tilde denotes quantities normalized by μ. Λ is a factor that is determined by the normalization condition of the density. For a discrete surface, in order to observe the average behavior, $\int\int_{L_x,L_y} d^2\tilde{r}\,\tilde{n}(\tilde{r})/(L_xL_y)$ was calculated. When dielectric discontinuity is present, however, the potential cannot be written simply as $1/r$. It should be represented as an infinite series of summations of image charges. The results of pure $1/r$ contribution formulas definitely differ from the numerical results. For a more relevant comparison, the surface contributions are extended not only to the macroion itself but also to all of its image charges. Although the replicated image of macroions could be accounted for as a summation of images whose strength decays proportionally to ϵ_{21}, the images of counterions, which yield a repulsive contribution, are difficult to incorporate. Figure 4 shows that strong-coupling theory agrees well with the numerical results when $\epsilon_1=79$, but it gives quite different results in other ranges. Nonetheless, counterions are still localized to surfaces. Figure 4 shows that the localization of counterions as predicted by the strong-coupling theory is far greater than in the numerical results for a low dielectric constant of the surface medium.

In this model, the counterion radius is important. It determines not only the interface where image charges are generated, but also the minimal distance between real charges and their images. The minimal distance between counterions and surfaces is set to the counterion radius r_c. The center of the counterions can be distributed from 0 to d. In agreement with this, the reflection interfaces are located at $z=-r_c$ and $d+r_c$. Figure 5 shows the counterion density profile as a function of the surface charge radius. As the counterion radius increases, which means as D/r_c decreases, the density at the surface, $n(0)$, also increases. This is because the image charge interaction decreases as the counterion radius becomes larger. When the radius is small enough, as shown in Fig. 5, $r_c \leqslant D/3.5$, the charge density at the surface tends to zero, and the counterions are driven to the midplane by the image charge repulsion.

In order to determine how the phase varies, an additional degree of freedom is imposed, that is, the lateral movement of plates. The corresponding Monte Carlo trial step can be described as follows. It is assumed that the upper plate can be moved with respect to the lower plate, while the square structure of the plates is maintained. The relative deviation of the upper plate from the lower plate is then measured. The results show that the deviation of phase depends on the depth of the particle, the dielectric difference, and the distance between the surfaces, which affects the strength of the interaction between bulk counterions and surface charges. Figure 6 shows that the in-phase case is preferable when the interaction is large, since counterions with valence equal to 2 are associated with the two corresponding surface charges. However, as the distance increases, the thermal fluctuations be-

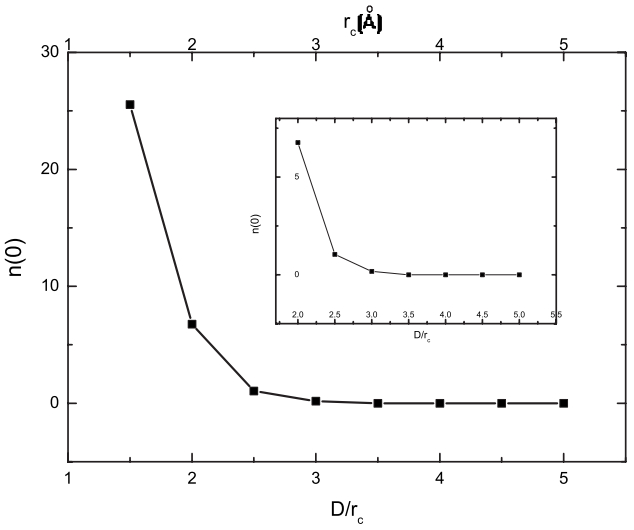

FIG. 5. Density ratio of counterions at midplane and at surfaces vs radius of counterion. Density at surface decreases with increasing radius of counterion. $\Xi=5$, $q=2$, $D/a_\perp=0.05$, $d/a_\perp=0.133$, $\epsilon_1=2$, and $\epsilon_2=79$.

come larger, and the corresponding deviation is not exactly zero, because the movement of the surfaces is assumed to preserve the canonical ensemble.

Figure 7 shows the results when the counterion valence is 1. Unlike the divalent case, there is a one-to-one association between surface charges and counterions in the monovalent case. The balance of interactions between surface charges and the corresponding bulk counterions determines the equilibrium behavior. Hence, it depends strongly on the depth, which corresponds to the minimum distance of interaction. With increased depth of surface charges, the association between surface charges and counterions is weakened, which means the counterions can deviate more from the corresponding surface charge location, and, as a consequence, the lateral correlation becomes weaker.

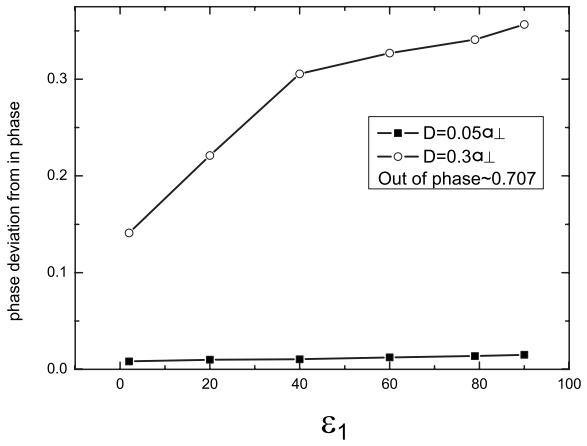

FIG. 6. Deviation of phase between two plates with lateral movement of plate. The in-phase case is preferred when depth is small and dielectric constant of the surface medium is small. $\Xi=5$, $q=2$, $D/a_\perp=0.05$, $r_c=D/3$, $d/a_\perp=0.133$.

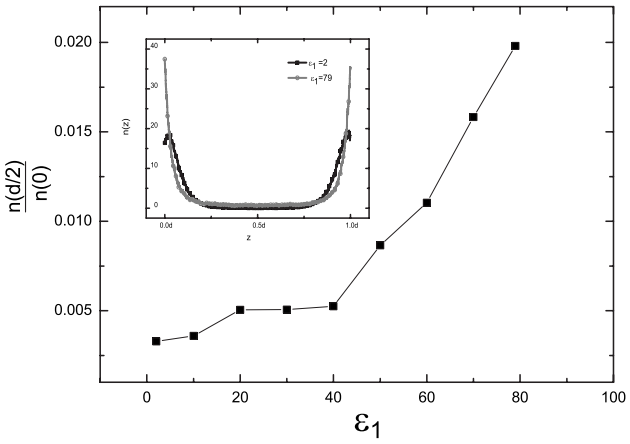

FIG. 7. Density ratio of counterions for monovalent case vs dielectric constant of surfaces. $\Xi=5$, $q=1$, $D/a_\perp=0.05$, $r_c=D/3$, $d/a_\perp=0.133$.

The density profile of counterions depends on the dielectric discontinuity in the monovalent case. It shows a different tendency from the profile in the divalent case. Owing to the one-to-one correspondence between surface charges and counterions, the localization phenomenon maintains even a large dielectric discontinuity. The density of counterions at the surface decreases, but that of counterions at the midplane also decreases with decreasing ϵ_1. As a result, the ratio $n(d/2)/n(0)$ becomes smaller with decreasing ϵ_1. This tendency is opposite to that of the divalent case, but the phenomenon that counterions are driven to the midplane still holds. It comes from the fact that the speed of density decay at the midplane is faster than that of density decay at the surface with decreasing ϵ_1. As seen from the inset of Fig. 7, counterions experience repulsion from the surface in the presence of a dielectric difference.

Figure 8 is a plot of the pressure between the two plates as a function of ϵ_1 both in and out of phase at $q=2$. This figure shows that the pressure in the in-phase case is smaller than that in the out-of-phase case. The same result is also valid for the case in which there is no dielectric discontinuity. The

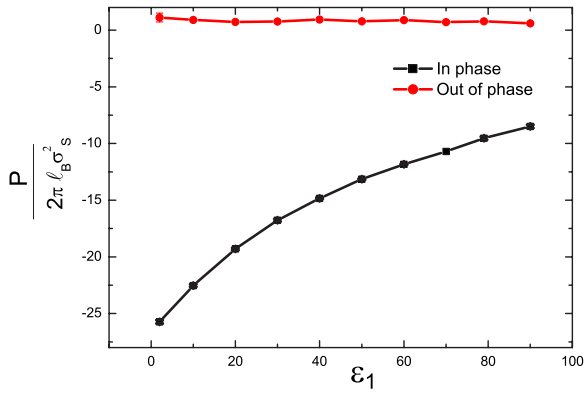

FIG. 8. (Color online) Pressure between two plates vs dielectric constant of the surface with divalent counterions. In particular, the pressure can be strongly attractive in the in-phase case. $\Xi=5$, $q=2$, $D/a_\perp=0.05$, $r_c=D/3$, $d/a_\perp=0.133$.

divalent counterions mediate the attraction by interacting simultaneously with two corresponding surface charges. The relevant attraction is stronger for the in-phase than the out-of-phase case. This is true as long as the lateral distance of the macrocharges is much larger than the vertical z distance. In general, a real system belongs to the strong-coupling regime, and the distance between surface charges and counterions is much smaller than the lateral distance between particles; in this case, $D/a_\perp=0.05$, $d/a_\perp=0.133$.

If there is no dielectric discontinuity in the in-phase structure, the strong attraction can be attributed to the localization of counterions since the localization involves a strong correlation between counterions, surface charges, and the associated strong attraction between them. However, for situations involving dielectric discontinuity, somewhat different results are obtained. The localization of counterions to the surface becomes weaker for a smaller dielectric constant ϵ_1 of the surface; nonetheless, the pressure becomes stronger for smaller ϵ_1 (it is eight times stronger when ϵ_1 is 2 than when ϵ_1 is 79). The pressure is composed of four types of interaction: interactions between counterions, between counterions and surface charges, and between surface charges, and the entropic pressure of counterions.

At equilibrium, the pressure is expected to be the same at all points between the two plates. For the interface, in comparison with the nondielectric discontinuity case, the four pressure corrections can be described as follows. The interaction between counterions contributes to the repulsion because of image charges. However, the interaction between the counterion and surface charge contributes to attraction. The Coulomb interaction between two different media is proportional to $2/(\epsilon_1+\epsilon_2)$, which is greater than $1/\epsilon_2$. For the case $\epsilon_1=2$, $\epsilon_2=79$, the interaction between different media is greater than 1.95 times that between the same media. Moreover, same-sign-images amplify this attraction. The interaction between surface charges is repulsive, but it decays as the distance between the plates increases, and is smaller compared to the attractive contribution. The entropic pressure is apparently less repulsive because counterions are driven to the midplane. On the whole, the net pressure becomes more attractive with decreasing ϵ_1. The results for the out-of-phase case are distinctly different from those in phase: contrary to the in-phase case, the pressure becomes more repulsive as ϵ_1 decreases. This can be understood because the lateral correlation is weaker than in the in-phase case. Hence, the repulsive contribution due to the same-sign image charge overcomes the attraction between the surface charges and counterions.

The pressure also has a dependence on the radius ratio of the counterions and surface charges. Figure 9 shows that, as the radius is decreased, the minimum distance of interaction becomes smaller.

For the monovalent case shown in Fig. 10, the pressure between the two plates shows a more drastic change. In the case of no dielectric discontinuity, the pressure was repulsive. (For the monovalent case, the attraction between the surface and counterion is smaller than in the divalent case, and the net pressure is mostly repulsive [9].) However, considering the dielectric discontinuity, it can become attractive, as Fig. 10 shows. This result originates from the fact that the

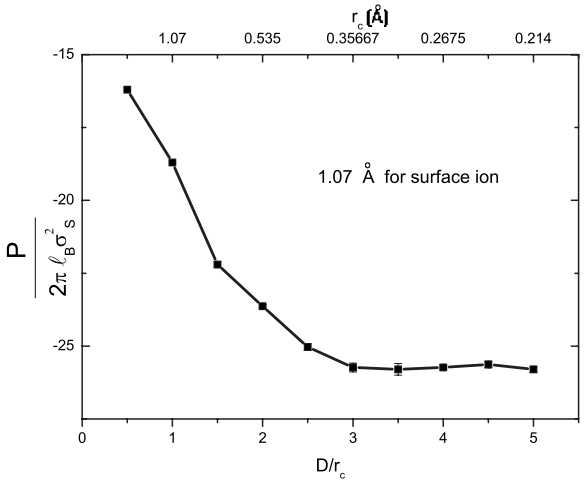

FIG. 9. Pressure between two plates vs radius of counterion. With decreasing radius of the counterion, the pressure becomes more attractive. $\Xi=5$, $q=2$, $D/a_\perp=0.3$, $r_c=D/3$, $d/a_\perp=0.133$.

surface charges in a low dielectric medium give rise to a higher electrostatic attraction. As the dielectric constant of the surface medium is decreased, the pressure becomes lower; in particular, for the system conditions of Fig. 10 the pressure turns negative when the dielectric constant of the surface medium becomes less than 20 in these simulation conditions.

IV. DISCUSSION AND CONCLUSION

Compared to the case of no dielectric discontinuity, there are two significant differences when dielectric discontinuity is considered. One is the stronger association between surface charges and bulk counterions, which comes from the low dielectric constant of the surface medium compared to that of water. The other is the repulsive interaction that counterions experience from their image charges generated at the interfaces. The interaction between counterions and their im-

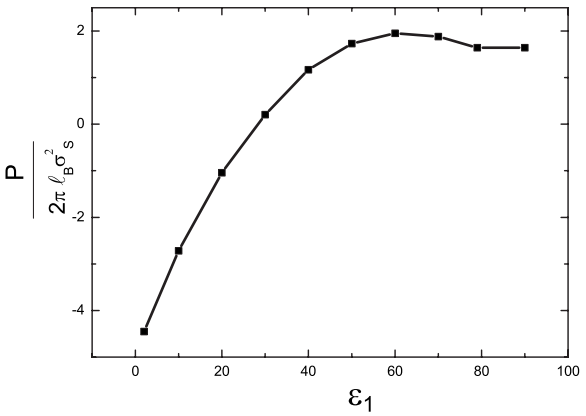

FIG. 10. Pressure between two plates for monovalent case. Pressure can be attractive for a low dielectric surface even though it is repulsive if the dielectric constant of the surface is high. $\Xi=5$, $q=1$, $D/a_\perp=0.05$, $r_c=D/3$, $d/a_\perp=0.133$.

age charges depends on the dielectric constant of the two media. If the dielectric constant of the bulk medium is greater than that of the surface medium, a repulsive interaction occurs, and vice versa. For a conventional biosystem, where the bulk medium consisting of water is highly dielectric compared to the surrounding surfaces, this observation signifies that the repulsive interaction between bulk counterions and image charges is substantially enhanced. For this reason, counterions become more strongly driven to the center of the bulk medium when the dielectric difference is higher; otherwise, they are more localized to the surface. With regard to the pressure between the two plates, it can be seen that a low dielectricity of the surface medium, which equates to less shielding of the electrostatic interaction, tends to induce more attraction between the plates.

ACKNOWLEDGMENT

During this work, Y.S.J. and M.W.K. were supported by Korean KISTEP under Grant No. I-03-064 and a grant from the Korea Health 21 R&D Project; G.P. and C.S.C. were supported by the Korean Basic Science Institute; and P.A.P. and M.W.K. were supported by the National Science Foundation Grant No. DMR-0503347.

[1] R. R. Netz, Eur. Phys. J. E **5**, 557 (2001).
[2] A. G. Moreira and R. R. Netz, Eur. Phys. J. E **8**, 33 (2002).
[3] A. W. C. Lau and P. Pincus, Phys. Rev. E **66**, 041501 (2002).
[4] B. I. Shklovskii, Phys. Rev. E **60**, 5802 (1999).
[5] Hiroshi Frusawa, J. Phys. Soc. Jpn. **73**, 507 (2004).
[6] Z. Donko and G. J. Kalman, Phys. Rev. E **63**, 061504 (2001).
[7] S. A. Safran, *Statistical Thermodynamics of Surfaces, Interfaces, and Membranes* (Addison-Wesley, Reading, MA, 1994).
[8] I. Rouzina and V. A. Bloomfield, J. Phys. Chem. **100**, 9977 (1996).
[9] Y. S. Jho, G. Park, C. S. Chang, P. Pincus, and M. W. Kim, Phys. Rev. E **73**, 021502 (2006).
[10] R. Menes, P. Pincus, and B. Stein, Phys. Rev. E **62**, 2981 (2000).
[11] A. G. Moreira and R. R. Netz, Europhys. Lett. **52**, 705 (2000).
[12] T. T. Nguyen, A. Yu. Grosberg, and B. I. Shklovskii, J. Chem. Phys. **113**, 1110 (2000).
[13] T. T. Nguyen and B. I. Shklovskii, Phys. Rev. E **64**, 041407 (2001).
[14] R. R. Netz and J. F. Joanny, Macromolecules **32**, 9013 (1999).
[15] R. R. Netz and J. F. Joanny, Macromolecules **32**, 9026 (1999).
[16] D. Andelman and J. F. Joanny, C. R. Acad. Sci., Ser IV: Phys., Astrophys. **1**, 1153 (2000).
[17] G. Iversen, Y. I. Kharkats, and J. Ulstrup, Mol. Phys. **94**, 297 (1998).
[18] J. D. Jackson, *Classical Electrodynamics*, 3rd ed. (Wiley, New York, 1998).
[19] A. Arnold and C. Holm, Comput. Phys. Commun. **148**, 327 (2002).
[20] A. Arnold, J. Joaniss, and C. Holm, J. Chem. Phys. **117**, 2496 (2002).
[21] A. Arnold, Ph.D. thesis, MPI für Polymerforschung, 2004.
[22] D. Frenkel and B. Smit, *Understanding Molecular Simulation* (Academic, San Diego, 1996).
[23] Y. Aoyama and J. Nakano, *RS/6000SP: Practical MPI Programming* (IBM Redbooks, Japan, 1999).